ADVANCED ENERGY & SUSTAINABILITY RESEARCH
Open Access
www.advenergysustres.com

Near-Atomic-Scale Evolution of the Surface Chemistry in Li[Ni,Mn,Co]O_2 Cathode for Li-Ion Batteries Stored in Air

Mahander P. Singh, Se-Ho Kim, Xuyang Zhou, Hiram Kwak, Alisson Kwiatkowski da Silva, Stoichko Antonov, Leonardo Shoji Aota, Chanwon Jung, Yoon Seok Jung, and Baptiste Gault**

Layered $LiMO_2$ (M = Ni, Co, Mn, and Al mixture) cathode materials used for Li-ion batteries are reputed to be highly reactive through their surface, where the chemistry changes rapidly when exposed to ambient air. However, conventional electron/spectroscopy-based techniques or thermogravimetric analysis fails to capture the underlying atom-scale chemistry of vulnerable Li species. To study the evolution of the surface composition at the atomic scale, cryogenic atom probe tomography is used herein and the surface species formed during exposure of a $LiNi_{0.8}Mn_{0.1}Co_{0.1}O_2$ (NMC811) cathode material to air are probed. The compositional analysis evidences the formation of Li_2CO_3. Site-specific examination from a cracked region of an NMC811 particle also reveals the predominant presence of Li_2CO_3. These insights will help to design improved protocols for cathode synthesis and cell assembly, as well as critical knowledge for cathode degradation.

During storage in air under ambient conditions of temperature and pressure, the high surface reactivity of Ni-rich layered oxide cathode materials used in rechargeable Li-ion battery leads to the generation of certain surface species, which causes problems during electrode slurry preparation, cell storage, and charge/discharge cycling.[1–3] For example, Jung et al.[4] showed that ambient storage of Ni-rich $LiNi_xMn_yCo_{1-x-y}O_2$ (NMC) cathode for a year led to significant surface contamination. The authors suggested a possible formation of Ni carbonate species, making the particles electrochemically inactive with severely degraded electronic conductivity and hindered Li transport. Eventually there was considerable impedance growth and irreversible capacity loss. In another report, Busa et al.[5] reported that NMC particles exposed to humid air for 28 days showed an increase of capacity over the first 25 cycles, suspected to be due to the decomposition of possible lithium carbonates formed during air exposure, followed by a dramatic capacity fade of 70%, whereas the pristine sample exhibited a stable cycling performance (98% capacity retention). Archival literature suggests possible formation of lithium/nickel hydroxides, oxides, and carbonates during air/moisture interaction with NMC surfaces at near room temperatures.[4,6] The chemical composition of the surface species is very important in terms of electrical resistance and Li-ion transport. However, the actual atomic-scale chemistry of Ni-rich oxide cathode materials after exposure to air or moisture remains elusive (nickel vs lithium carbonate/hydroxides/oxides). Yet, it impacts battery operation, lifetime, and the formation and chemistry of the cathode–electrolyte interphase which are subjects of intensive research efforts.[7–9] Elucidating the surface reactions will ultimately allow for improved understanding of the degradation pathways and underpin its solutions.

The chemical and structural evolution of the cathode–air interface is challenging to image and is mostly studied by electron/spectroscopy-based techniques or thermogravimetric analysis. Spatially resolved techniques such as scanning/transmission electron microscopy (SEM/TEM) are widely applied to address the surface degradation phenomenon. However, Li-based compounds are susceptible to electron beam damage, which complicates data interpretation.[10–13] Similarly, X-ray illumination of Li containing compounds forces an uncontrollable evolution toward stable lithium oxide, even in the soft X-ray regime, precluding safe and reliable application of X-ray-based spectroscopy techniques.[14–17] Alternative analytical techniques are now being

M. P. Singh, S.-H. Kim, X. Zhou, A. Kwiatkowski da Silva, L. S. Aota, C. Jung, B. Gault
Department of Materials Physics and Alloy Design
Max-Planck-Institut für Eisenforschung
40237 Düsseldorf, Germany
E-mail: s.kim@mpie.de; b.gault@mpie.de

H. Kwak, Y. S. Jung
Department of Chemical and Biomolecular Engineering
Yonsei University
Seoul 03722, South Korea

S. Antonov
Materials Engineering and Manufacturing Directorate
National Energy Technology Laboratory
1450 Queen Ave SW, Albany, OR 97321, USA

B. Gault
Department of Materials
Royal School of Mines
Imperial College London
London SW72AZ, UK

The ORCID identification number(s) for the author(s) of this article can be found under https://doi.org/10.1002/aesr.202200121.

DOI: 10.1002/aesr.202200121

explored to circumvent these issues. Time-of-flight secondary ion mass spectrometer (TOF-SIMS) and atom probe tomography (APT) which provides quantitative, analytical 3D imaging with subnanometer resolution are currently the most suitable solutions.[18,19]

Here, we use APT, complemented by cryogenic electron- and ion-microscopy techniques,[20] to track the morphological and compositional evolution of the surface of $Li(Ni_{0.8}Mn_{0.1}Co_{0.1})O_2$ (NMC811) particles, a commercial cathode material, over increasing storage time under ambient air conditions. These insights aid to further understand the relationship between surface chemistry and electrochemical performance upon air ambient storage, thus helping to rationalize storage periods or air ingress during manufacturing.

We recently demonstrated that the APT analysis of pristine NMC811, following specimen preparation by focused-ion beam (FIB) milling at room temperature, was enabled by slight compositional changes of the surface when transferred through air, under ambient lab conditions,[19] as shown in **Figure 1**a. The real space 3D atom map of the as-received pristine NMC811 in

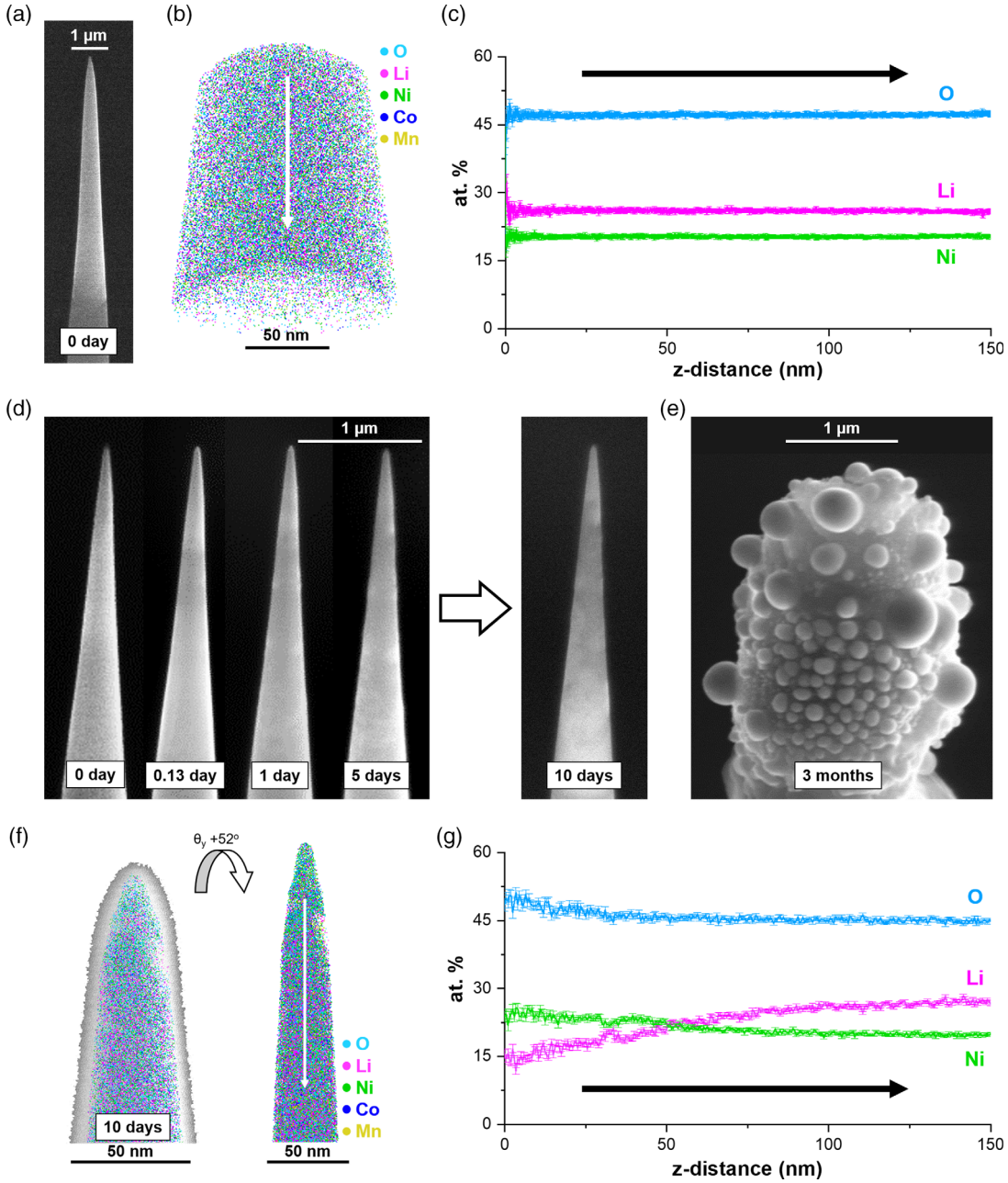

Figure 1. a) SEM image and b) 3D atom map of NMC811 APT specimen. c) Corresponding 1D atomic compositional profile along the measurement direction (white arrow in (b)). d) Ex situ oxidation experiment at different time span. e) NMC specimen after 3 month oxidation in ambient condition. f) APT specimen after 10 days oxidation and electron beam exposure for imaging. Inset image shows 3D atom map results with tilted at 52° in *y*-axis. g) Corresponding 1D atomic compositional profile along the measurement direction (white arrow in (f)). Co and Mn elements are not shown.

Figure 1b shows no substantial chemical fluctuation, as quantified by the composition profile in Figure 1c. Note that the O atomic concentration is lower than the nominal NMC composition, which can be attributed to the dissociative processes of molecular ions leading to species-specific losses.[21,22]

A series of similar APT specimens were prepared and analyzed by APT, in order to clean their surface of possible damage from the specimen preparation. These specimens were then exposed to air and imaged with the SEM at intermediate times (Figure 1d and S1, Supporting Information). The change in contrast suggests a progressive change in the underlying microstructure. Upon exposure to ambient air for 3 months, protrusions on the side of the needle-shaped specimen formed, Figure 1e, precluding its analysis; it immediately fractured once we applied voltage on specimen due to the uneven surface morphology. APT analysis after 10 day exposure, Figure 1f–g, contrasts with the pristine material. The air exposure leads to a redistribution of Li and a change in the Li:Ni ratio toward the specimen's surface, either toward the apex, Figure 1g, or toward the sides, Figure S2, Supporting Information, with the formation of Li-depleted region, yet no carbonate species was detected, which indicates the layer is not a nickel carbonate species.[4]

This poses the important question of where does the surface Li go? Extreme caution is required when electron microscopy is used for characterizing Li materials as the electron beam can easily damage the structure and chemistry that could lead to misinterpretation of results.[13] To assess the influence of the electron beam illumination on the NMC811 during SEM imaging on the quantification of this elemental redistribution, we cross-sectioned with the FIB a NMC811 particle with the FIB, and exposed it to air for a month. Both the external surface and cross-sectioned of air-aged NMC particles get covered with similar precipitates (Figure S3, Supporting Information), implying that possible damage from the FIB during preparation did not change the nature of the reaction in air even if its kinetic may have been affected by the presence of structural damage. Even using a low acceleration electron beam voltage of 5 kV, at relatively low electron beam current of 0.6 nA, a short exposure of 5 s in the SEM led to critical irradiation damage to the surface layer (**Figure 2** and S3, Supporting Information). The same behavior was observed when we illuminated the electron beam on the surface-oxidized NMC 811 particle under TEM as it immediately reacted with the material (see Figure S4, Supporting Information).

To analyze these beam-sensitive layers, we introduce a workflow that minimizes the degradation from the illumination by the electron beam necessary during imaging and specimen preparation. We first cross-sectioned an NMC particle with the FIB, **Figure 3**a, during which electron beam usage was minimized and limited only to low magnification so as it is not concentrated in a certain region/particle. The cut NMC811 particles were then exposed to air for a month. A thick Cr film (≈200 nm) was then deposited by physical vapor deposition (PVD), as detailed in Figure S5–S7, Supporting Information, in order to protect the reacted core surface region from beam damage. Note that the Cr layer was thin enough to clearly discern the features of the particles, yet thick enough to protect their surfaces from electron beam damage. APT specimens from these coated particles were then prepared at room temperature followed by sharpening at cryogenic temperature using the protocol outlined in ref. [23]. Figure 3b shows the corresponding 3D atom map, and underneath the Cr cap is a carbon-rich region, with a ratio of Li to C of ≈2, consistent with Li_2CO_3 (see composition in Table S1, Supporting Information), followed by a gradient Li-depleted NMC region (NiO-like impurity), as quantified by the composition profile in Figure 3c.

Interestingly, the formation of a NiO layer has been reported by a parasitic side reaction with the electrolyte during the cell cycles;[24,25] however, here we demonstrate that exposing in air already has created a NiO layer covered by the carbonate. Co and Mn distributions are plotted in Figure S8, Supporting Information, and they are present along with the Ni signal. As the Li_2CO_3 layer is very sensitive under electron beam, it is easily

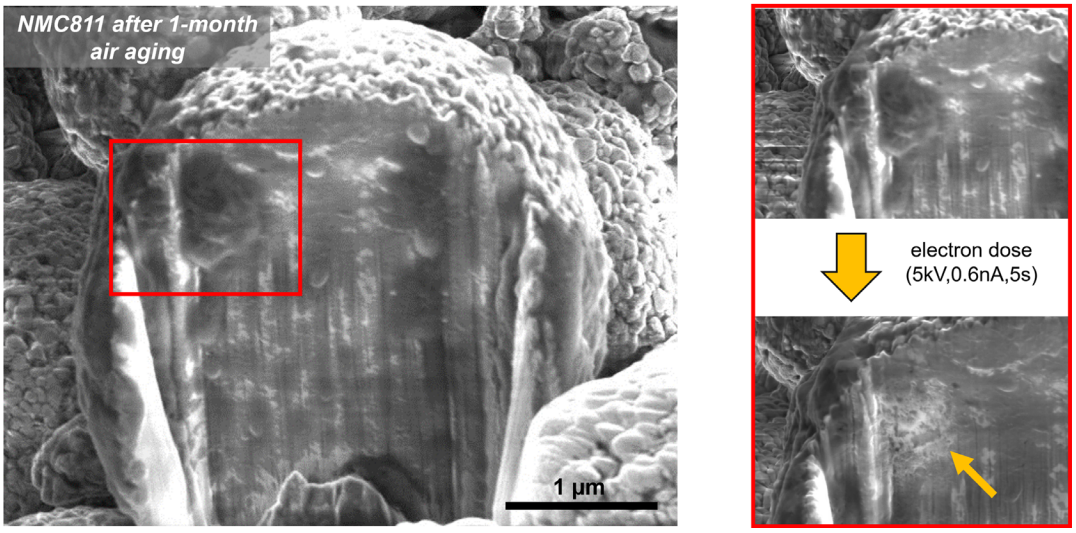

Figure 2. Electron beam-induced decomposition of Li_2CO_3 layers on air-aged NMC particle. Yellow arrow remarks the deformation induced by electron beams. Additional information is shown in Figure S3, Supporting Information.

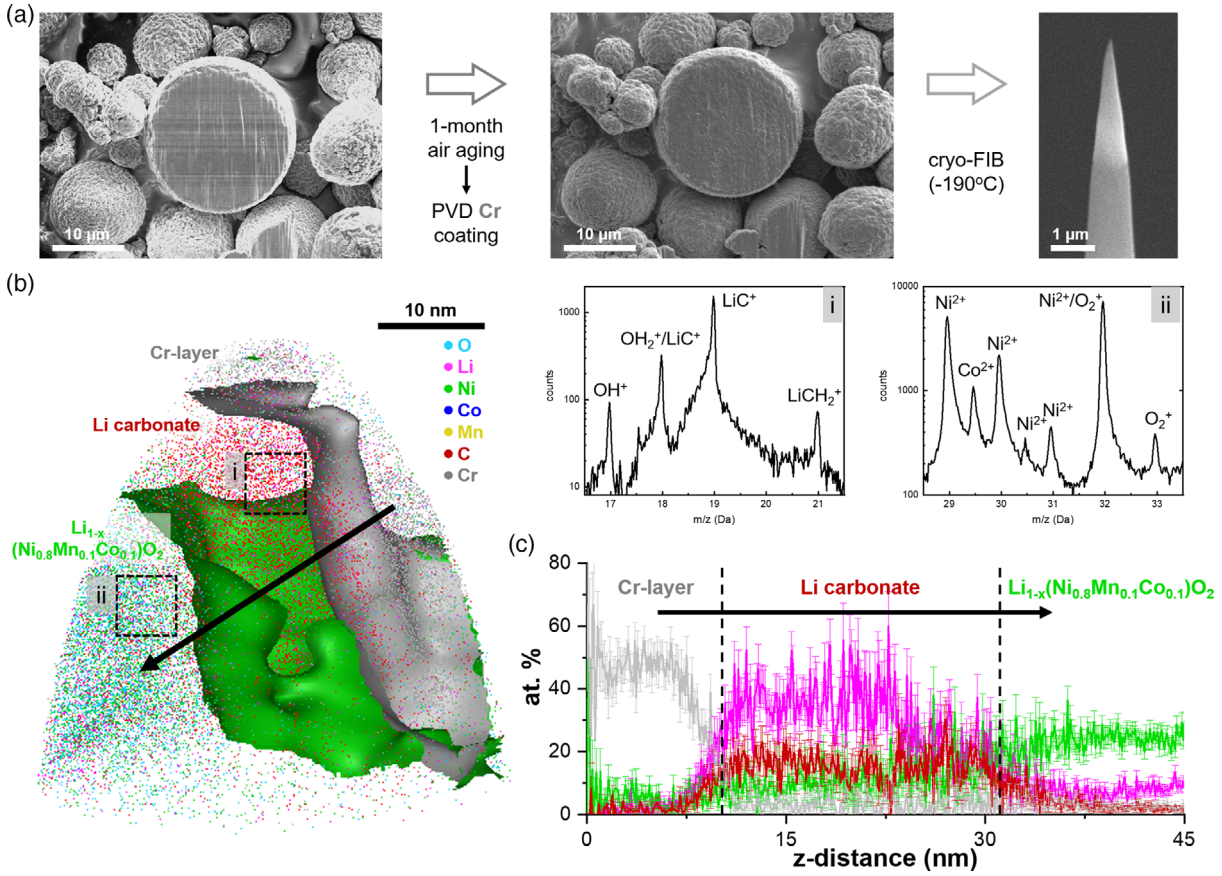

Figure 3. Atomic chemistry analysis of a month oxidized NMC particle. a) The APT specimen preparation of surface-sensitive material with PVD coating and cryogenic milling. No electron beam imaging was done before the PVD-Cr coating and 1 month ambient storage. b) 3D atom map of Cr-coated oxidized NMC surface. Inset i and ii display extracted local mass spectra of interest regions in (b). In the extracted mass spectrum of the impurity layer, it indeed shows the peak of Li–C molecular ions that we can conclude the presence of Li_2CO_3. c) 1D compositional profile of elements across the oxidized NMC surface (cylindrical region of interest of $\Phi 5 \times 50\,nm^3$). Co, Mn, and O elements are not plotted. The details of the mass spectrum analysis are presented in Figure S9, Supporting Information.

removed when observed, hence it was not seen in the APT data after oxidation in Figure 1, and we were able to observe the remaining Li-depleted Ni-rich oxide layer. The inhomogeneity of the surface structure of air-exposed NMC sample has not been previously reported and discussed in any APT analysis paper on Li-ion batteries.[18,19,26–28] This could be due to its elimination during imaging as previously mentioned, the limited field of view of current atom probe system,[29] and the loss of the material during first laser alignment to the detector and the specimen.[30] Conversely, when the prerun specimen was left in ambient air for 4 h and resumed the measurement without electron beam imaging, hydroxyl ions appear to be adsorbed on its surface.[31]

Although substantial Li ions diffuse onto the NMC surface, the Li composition in the NMC does not vary much as the NMC is an abundant Li reservoir. Approximately 1 µm below the top surface, following further milling in the FIB after 1 month oxidation, the elemental distribution is back to what was measured in the pristine sample (see Figure S10, Supporting Information). The core of the sample shows a homogeneous elemental distribution with similar composition to the initial sample, suggesting that the inner structure and chemistry would not be influenced much from air oxidation in APT measurement.

In the reactive environment, the strong affinity between Li and gases in the reactive environment results in Li-ion migration toward the surface where it reacts with gaseous species. In situ, environmentally controlled TEM recently revealed a successive reaction of NMC cathode materials with water (i.e., moisture in air), leading to the formation of a LiOH layer on the surface.[32] A strong driving force for Li migration to form LiOH explains the Li concentration gradients found in Figure 3c. LiOH spontaneously reacts with CO_2 at room temperature to form Li_2CO_3 ($\Delta G = -88\,kJ\,mol^{-1}$).[33] This reaction explains the use of LiOH canisters for CO_2 removal in space shuttles.[34] However, Li_2CO_3 is a wide bandgap insulator that acts as a passivation layer to slow the electrode–electrolyte because of sluggish electrons transport. It exhibits extrinsic conduction, essentially by electromobility of interstitial Li ions,[35] yet it can act as a barrier against chemical delithiation, and its presence results in inferior reversibility and cyclability.[36] Moreover, Li_2CO_3 can seriously damage a battery package when the common electrolyte salt ($LiPF_6$) is used through the following

reaction:[37] $LiPF_6 + Li_2CO_3 \rightarrow POF_3\uparrow + CO_2\uparrow + 3LiF$. The carbonate attacked by the salt generates gaseous products (POF_3 and CO_2) which cause swelling inside a package and decrease the active surface site from gas adsorption gradually aggregating the cell's polarization.[38,39]

As Li_2CO_3 impurity cannot be well controlled in current practical application, besides heat and washing treatments[37,40] after the cathode synthesis for Li_2CO_3 removals, a simple approach to improve the high-Ni cathode performance and life is to keep extremely CO_2 levels low. The atmosphere air contains roughly 400 ppm_v and this low content already induced abrupt Li_2CO_3 formation on the cathode surface (see Supporting Information for the threshold CO_2 level). Generally, an inert gas-filled glove box has a sensor for O_2/H_2O but not CO_2,[41] whereas controlling its level appears crucial to the quality of the NMC during synthesis and assembly.

Preexisting intragranular cracks from the synthesis have been considered to be one of the major degradation mechanisms,[42,43] assisting with the build-up of stresses and strains during the phase transition and potentially assisting with chemical reactions with the electrolyte or nucleation of new phases.[9,42,44] These cracks are serious concern while operating batteries at higher voltages. Surface coatings of cathode particles have been shown to provide efficient protective layer to hinder the dissolution of the constituent metal from the particles, and enhance the internal structure stability,[45,46] yet the precise mechanisms by which coatings interact with preexisting or freshly formed cracks cannot yet be discussed without a dedicated future study.

We exposed a crack-containing NMC811 particle to air and, in **Figure 4**a, the red arrow indicates a region where the crack swelled, while a different phase has grown on its surface that the APT analysis in Figure 4b reveals to be also Li_2CO_3. When exposed to air environment, the fresh surface created by the propagating crack triggers further phase transformation into a carbonate, which induces Li diffusion and consequently leads to locally lower electrical conductivity and internal Li-ion mobility, accelerating high resistivity of the cathode.[42,47] Furthermore, the resultant carbonate channel inside the particles can be attacked by the electrolyte and accelerates the formation of NiO-like impurity, eventually leading to structural degradation and an inferior rate capability and kinetic loss of capacity.[48]

Our findings point to four distinguishable layers formed on the Ni-rich oxide cathode particle stored in ambient conditions: a Li-carbonate, a Li-depleted layer, likely to be a 2 nm-thick rock-salt (Ni–O like) shell previously observed by in situ TEM,[32] a lithium diffusion (Ni-rich) layer, and finally the pristine NMC811 phase. Each individual region will have a different composition and possibly structure, and hence impedance, which,

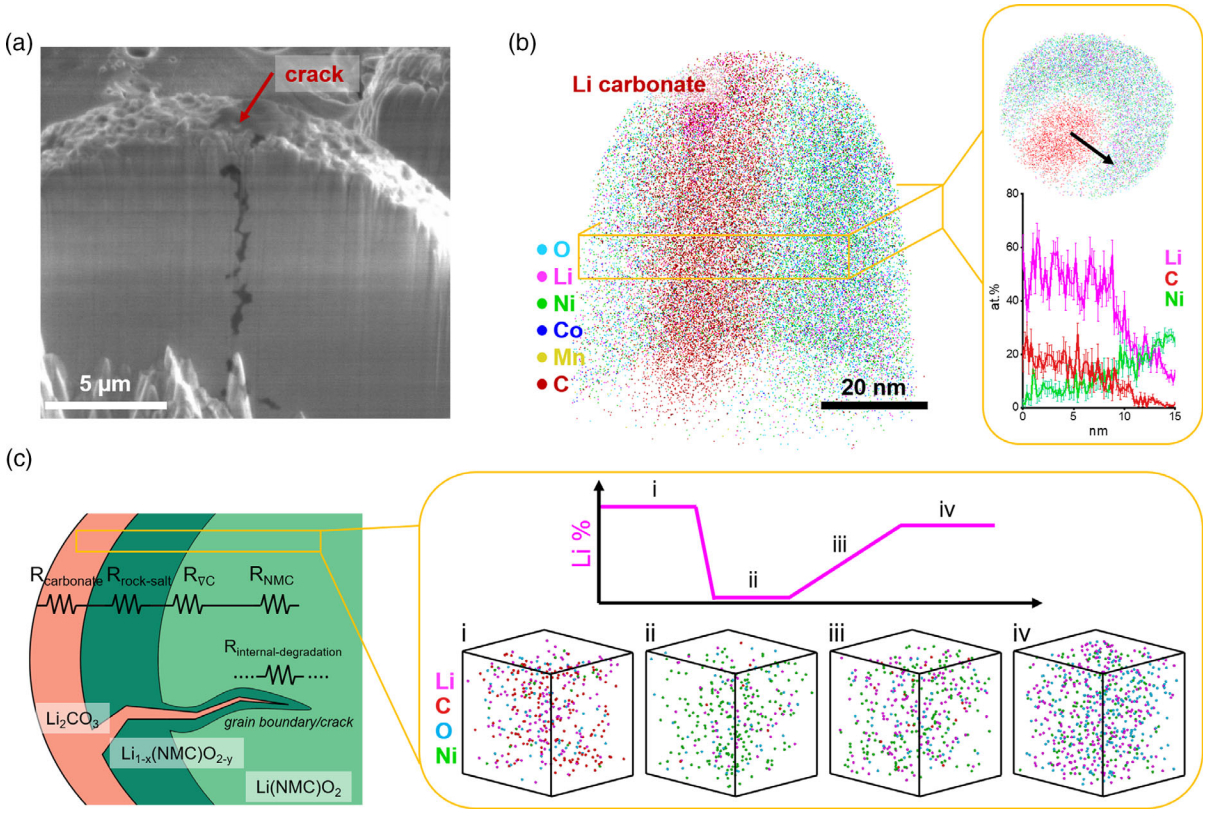

Figure 4. a) Cross-sectioned air-stored NMC particle. b) APT result of the NMC with Li_2CO_3. The specimen was prepared by the non-cryo protocol. The orange box shows (top) the 5 nm-thin-sliced tomogram along the APT measurement direction and (bottom) atomic compositional profile at the interface marked by the black arrow in the tomogram. c) A schematic illustration of NMC 811 material after air oxidation with an arbitrary Li concentration profile along the surface. Note that the insets show the extracted cuboidal volume ($3 \times 3 \times 3$ nm^3) of each different layer: Li_2CO_3, Ni-rich oxides, diffusion profile, and NMC particles. Pink, red, blue, and green spheres represent the reconstructed Li, C, O, and Ni atoms. Additionally, Figure S11, Supporting Information, shows many air-susceptible sites for NMC particles: grain boundaries, cracks, triple junction, surface, etc.

therefore, must be considered to fully comprehend the critical capacity loss of Ni-rich cathode materials. Figure 4c provides a schematic of inhomogeneous Li distribution from the formation of different phases under air exposure and their respective resistivity.

In summary, we systematically investigated the atomic-scale compositional evolution of Ni-rich NMC811 cathode powder exposed to ambient air. Extreme care should be taken to control, i.e., limit, exposure to electron beams from what of the products formed when testing and studying batteries materials. By adopting a cryogenic APT specimen preparation technique for the electron beam sensitive Li compounds, we carefully confirm Li-ion extraction from the particles driven by the formation of LiOH that reacts with CO_2 in air to form Li_2CO_3 and creates a local Li and Ni concentration gradient along the surface. Beyond the surface of individual particles, the surface of cracks from synthesis or arising from the volume change during the charge/discharge cycles are also covered with Li_2CO_3, thereby increasing internal stresses, and further contributing to facilitate the nucleation and/or growth of stress corrosion cracks. Although the changes we image are on a scale of only tens of nanometers or below, the associated differences in Li-ion mobility and impendence can induce high initial voltage peak upon delithiation in the first charge and irreversible capacity loss.[4,49] Alleviating the formation of different phases by minimizing the encounter with air or other reactive species should be prioritized, in order to prevent the formation of inhomogeneity in the Li distribution before and during cycling to retain a stable charge and discharge performance over the course of the battery lifetime.

Supporting Information

Supporting Information is available from the Wiley Online Library or from the author.

Acknowledgements

S.H.K. and B.G. are grateful for financial support from the ERC-CoG-SHINE-771602 at some point in the last few years. S.H.K. and B.G. acknowledge financial support from the DFG through the DIP Project number 450800666. S.A. and X.Z. are grateful for financial support from the Alexander von Humboldt Foundation.

Open Access funding enabled and organized by Projekt DEAL.

Conflict of Interest

The authors declare no conflict of interest.

Data Availability Statement

The data that support the findings of this study are available from the corresponding author upon reasonable request.

Keywords

ambient oxidation, atom probe tomography, Li-ion batteries, NMC cathodes

Received: August 8, 2022
Revised: November 15, 2022
Published online: November 27, 2022

[1] M. Bichon, D. Sotta, N. Dupré, E. De Vito, A. Boulineau, W. Porcher, B. Lestriez, *ACS Appl. Mater. Interfaces* **2019**, *11*, 18331.
[2] J. Eom, M. G. Kim, J. Cho, *J. Electrochem. Soc.* **2008**, *155*, A239.
[3] K. Shizuka, C. Kiyohara, K. Shima, Y. Takeda, *J. Power Sources* **2007**, *166*, 233.
[4] R. Jung, R. Morasch, P. Karayaylali, K. Phillips, F. Maglia, C. Stinner, Y. Shao-Horn, H. A. Gasteiger, *J. Electrochem. Soc.* **2018**, *165*, A132.
[5] C. Busà, M. Belekoukia, M. J. Loveridge, *Electrochim. Acta* **2021**, *366*, 137358.
[6] R. Moshtev, P. Zlatilova, S. Vasilev, I. Bakalova, A. Kozawa, *J. Power Sources* **1999**, *81–82*, 434.
[7] Y. Wu, X. Liu, L. Wang, X. Feng, D. Ren, Y. Li, X. Rui, Y. Wang, X. Han, G.-L. Xu, H. Wang, L. Lu, X. He, K. Amine, M. Ouyang, *Energy Storage Mater.* **2021**, *37*, 77.
[8] Z. Zhang, J. Yang, W. Huang, H. Wang, W. Zhou, Y. Li, Y. Li, J. Xu, W. Huang, W. Chiu, Y. Cui, *Matter* **2021**, *4*, 302.
[9] P. Yan, J. Zheng, J. Liu, B. Wang, X. Cheng, Y. Zhang, X. Sun, C. Wang, J. G. Zhang, *Nat. Energy* **2018**, *3*, 600.
[10] H. Zheng, Y. Liu, S. X. Mao, J. Wang, J. Y. Huang, *Sci. Rep.* **2012**, *2*, 542.
[11] R. F. Egerton, P. Li, M. Malac, *Micron* **2004**, *35*, 399.
[12] Y. H. Hu, E. Ruckenstein, *Chem. Phys. Lett.* **2006**, *430*, 80.
[13] F. Lin, I. M. Markus, M. M. Doeff, H. L. Xin, *Sci. Rep.* **2014**, *4*, 5694.
[14] A. Léon, A. Fiedler, M. Blum, A. Benkert, F. Meyer, W. Yang, M. Bär, F. Scheiba, H. Ehrenberg, L. Weinhardt, C. Heske, *J. Phys. Chem. C* **2017**, *121*, 5460.
[15] R. Qiao, Y. De Chuang, S. Yan, W. Yang, *PLoS One* **2012**, *7*, 3.
[16] M. Schellenberger, R. Golnak, W. G. Quevedo Garzon, S. Risse, R. Seidel, *Mater. Today Adv.* **2022**, *14*, 100215.
[17] B. T. Young, D. R. Heskett, J. C. Woicik, B. L. Lucht, *J. Spectrosc.* **2018**, *2018*, 1075902.
[18] A. Devaraj, M. Gu, R. Colby, P. Yan, C. M. Wang, J. M. Zheng, J. Xiao, A. Genc, J. G. Zhang, I. Belharouak, D. Wang, K. Amine, S. Thevuthasan, *Nat. Commun.* **2015**, *6*, 8014.
[19] S. Kim, S. Antonov, X. Zhou, L. Stephenson, C. Jung, A. El-Zoka, D. K. Schreiber, S. Conroy, B. Gault, J. Mater, S.-H. Kim, S. Antonov, X. Zhou, L. T. Stephenson, C. Jung, A. A. El-Zoka, D. K. Schreiber, M. Conroy, B. Gault, *J. Mater. Chem. A* **2022**, *6*, 4883.
[20] B. Gault, A. Chiaramonti, O. Cojocaru-Mirédin, P. Stender, R. Dubosq, C. Freysoldt, S. K. Makineni, T. Li, M. Moody, J. M. Cairney, *Nat. Rev. Methods Primers* **2021**, *1*, 51.
[21] D. W. Saxey, *Ultramicroscopy* **2011**, *111*, 473.
[22] B. Gault, D. W. Saxey, M. W. Ashton, S. B. Sinnott, A. N. Chiaramonti, M. P. Moody, D. K. Schreiber, *New J. Phys.* **2016**, *18*, 33031.
[23] L. Lilensten, B. Gault, *PLoS One* **2020**, *15*, 0231179.
[24] U.-H. Kim, H.-H. Ryu, J.-H. Kim, R. Mücke, P. Kaghazchi, C. S. Yoon, Y.-K. Sun, *Adv. Energy Mater.* **2019**, *9*, 1803902.
[25] S. Watanabe, M. Kinoshita, T. Hosokawa, K. Morigaki, K. Nakura, *J. Power Sources* **2014**, *258*, 210.
[26] D. Mohanty, B. Mazumder, A. Devaraj, A. S. Sefat, A. Huq, L. A. David, E. A. Payzant, J. Li, D. L. Wood, C. Daniel, *Nano Energy* **2017**, *36*, 76.
[27] J. Y. Lee, J. Y. Kim, H. I. Cho, C. H. Lee, H. S. Kim, S. U. Lee, T. J. Prosa, D. J. Larson, T. H. Yu, J. P. Ahn, *J. Power Sources* **2018**, *379*, 160.
[28] B. G. Chae, J. H. Lee, S. Park, E. Lee, C. M. Kwak, M. Jafari, Y. K. Jeong, C. G. Park, J. B. Seol, *ACS Nano* **2018**, *12*, 12109.
[29] M. Herbig, *Scr. Mater.* **2018**, *148*, 98.

[30] T. F. Kelly, M. K. Miller, *Rev. Sci. Instrum.* **2007**, *78*, 31101.
[31] S.-H. Kim, S. Antonov, X. Zhou, L. T. Stephenson, C. Jung, A. A. El-Zoka, D. K. Schreiber, M. Conroy, B. Gault, *J. Mater. Chem. A* **2022**, *10*, 4926.
[32] L. Zou, Y. He, Z. Liu, H. Jia, J. Zhu, J. Zheng, G. Wang, X. Li, J. Xiao, J. Liu, J. G. Zhang, G. Chen, C. Wang, *Nat. Commun.* **2020**, *11*, 3204.
[33] D. D. Williams, R. R. Miller, *Ind. Eng. Chem. Fundam.* **1970**, *9*, 454.
[34] J. Isobe, P. Henson, A. MacKnight, S. Yates, D. Schuck, D. Winton, in *46th Int. Conf. Environ. Syst.*, The Texas Tech University Libraries **2016**, pp. 10–14, https://ttu-ir.tdl.org/handle/2346/67727.
[35] X. Zhang, S. Weng, G. Yang, Y. Li, H. Li, D. Su, L. Gu, Z. Wang, X. Wang, L. Chen, *Cell Rep. Phys. Sci.* **2021**, *2*, 100668.
[36] B. D. McCloskey, A. Speidel, R. Scheffler, D. C. Miller, V. Viswanathan, J. S. Hummelshøj, J. K. Nørskov, A. C. Luntz, *J. Phys. Chem. Lett.* **2012**, *3*, 997.
[37] Y. Bi, T. Wang, M. Liu, R. Du, W. Yang, Z. Liu, Z. Peng, Y. Liu, D. Wang, X. Sun, *RSC Adv.* **2016**, *6*, 19233.
[38] A. Manthiram, J. C. Knight, S.-T. Myung, S.-M. Oh, Y.-K. Sun, *Adv. Energy Mater.* **2016**, *6*, 1501010.
[39] W. Liu, P. Oh, X. Liu, M.-J. Lee, W. Cho, S. Chae, Y. Kim, J. Cho, *Angew. Chem. Int. Ed.* **2015**, *54*, 4440.
[40] D. Pritzl, T. Teufl, A. T. S. Freiberg, B. Strehle, J. Sicklinger, H. Sommer, P. Hartmann, H. A. Gasteiger, *J. Electrochem. Soc.* **2019**, *166*, A4056.
[41] F. Friedrich, B. Strehle, A. T. S. Freiberg, K. Kleiner, S. J. Day, C. Erk, M. Piana, H. A. Gasteiger, *J. Electrochem. Soc.* **2019**, *166*, A3760.
[42] K.-J. Park, J.-Y. Hwang, H.-H. Ryu, F. Maglia, S.-J. Kim, P. Lamp, C. S. Yoon, Y.-K. Sun, *ACS Energy Lett.* **2019**, *4*, 1394.
[43] X. Fan, G. Hu, B. Zhang, X. Ou, J. Zhang, W. Zhao, H. Jia, L. Zou, P. Li, Y. Yang, *Nano Energy* **2020**, *70*, 104450.
[44] H. Park, H. Park, K. Song, S. H. Song, S. Kang, K.-H. Ko, D. Eum, Y. Jeon, J. Kim, W. M. Seong, H. Kim, J. Park, K. Kang, *Nat. Chem.* **2022**, *14*, 614.
[45] C. Liao, F. Li, J. Liu, *Nanomaterials* **2022**, *12*, 1888.
[46] Y. Shi, M. Zhang, D. Qian, Y. S. Meng, *Electrochim. Acta* **2016**, *203*, 154.
[47] H.-H. Ryu, K.-J. Park, C. S. Yoon, Y.-K. Sun, *Chem. Mater.* **2018**, *30*, 1155.
[48] N.-Y. Park, G.-T. Park, S.-B. Kim, W. Jung, B.-C. Park, Y.-K. Sun, *ACS Energy Lett.* **2022**, *7*, 2362.
[49] J. Sicklinger, H. Beyer, L. Hartmann, C. Sedlmeier, D. Pritzl, F. Riewald, H. A. Gasteiger, *ECS Meet. Abstr.* **2018**, *MA2018-02*, 235.